

ORIGINAL RESEARCH

Open Access

Uptake of ^{68}Ga gallium in atherosclerotic plaques in $\text{LDLR}^{-/-}\text{ApoB}^{100/100}$ mice

Johanna MU Silvola^{1*}, Iina Laitinen², Henri J Sipilä¹, V Jukka O Laine³, Pia Leppänen⁴, Seppo Ylä-Herttuala⁴, Juhani Knuti¹ and Anne Roivainen^{1,5}

Abstract

Background: Atherosclerosis is a chronic inflammatory disease of artery wall characterized by infiltration of monocytes into subendothelial space and their differentiation into macrophages. Since rupture-prone plaques commonly contain high amounts of activated macrophages, imaging of the macrophage content may provide a useful tool for the evaluation of plaque vulnerability. The purpose of this study was to explore the uptake of ^{68}Ga gallium (^{68}Ga) in atherosclerotic plaques in mice.

Methods: Uptake of ionic ^{68}Ga was investigated in atherosclerotic $\text{LDLR}^{-/-}\text{ApoB}^{100/100}$ and C57BL/6N control mice at 3 h after injection. The *ex vivo* biodistribution of the ^{68}Ga was assessed and autoradiography of aortic cryosections was defined. *In vivo* imaging of ^{68}Ga was performed using a small animal positron emission tomography PET/CT scanner.

Results: Our results revealed that the uptake of ^{68}Ga -radioactivity was higher in atherosclerotic plaques than in healthy vessel wall (ratio 1.8 ± 0.2 , $p = 0.0002$) and adventitia (ratio 1.3 ± 0.2 , $p = 0.0011$). The autoradiography signal co-localized with macrophages prominently as demonstrated by Mac-3 staining. In both mice strains, the highest level of radioactivity was found in the blood.

Conclusions: We observed a moderate but significantly elevated ^{68}Ga -radioactivity uptake in the aortic plaques of atherosclerotic mice, especially at the sites rich in macrophages. While the uptake of ^{68}Ga was promising in this animal model, the slow blood clearance may limit the usability of ^{68}Ga as a PET tracer for clinical imaging of atherosclerotic plaques.

Keywords: atherosclerosis, plaque, autoradiography, gallium-68, PET

Background

Atherosclerosis is a chronic inflammatory disease of artery wall with infiltration of monocytes into subendothelial space and their differentiation into macrophages. Macrophages express pro-inflammatory and chemotactic molecules thus playing an essential role in the formation, progression, and pathogenicity of atherosclerotic plaques. The population of macrophages in atherosclerotic lesions is heterogeneous. The majority of macrophages transform into foam cells by accumulating lipids in their cytoplasm, while other macrophages may have vascular protective and repair properties.

Furthermore, some macrophages may secrete enzymes that degrade the extracellular matrix and fibrous cap, possibly leading to a rupture of the atherosclerotic plaque. Significantly higher quantities of macrophage-rich plaque areas have been reported in atherosclerotic patients with acute coronary syndromes than in patients with stable angina. Since the rupture-prone plaques commonly contain high amounts of activated macrophages, imaging of the macrophages may provide a useful tool for determining plaque vulnerability [1-5].

^{68}Ga Gallium (^{68}Ga , $T_{1/2}$ 68 min) is a generator-produced, positron-emitting radionuclide with a high positron yield (89%) possessing suitable physical properties for *in vivo* PET imaging. ^{67}Ga Gallium (^{67}Ga) has traditionally been used to image inflammation with gamma cameras. Since ^{68}Ga owns the same chemical characteristics as ^{67}Ga , it is

* Correspondence: johanna.silvola@utu.fi

¹Turku PET Centre, University of Turku and Turku University Hospital, Turku, Finland

Full list of author information is available at the end of the article

assumed that ionic ^{68}Ga could accumulate at the sites of macrophage-rich areas in inflammatory lesions. Furthermore, ^{68}Ga -based PET may have some added advantages compared to ^{67}Ga -based SPECT, such as a better resolution for the detection of inflammatory plaques [6]. The aim of this study was to determine the uptake of ionic ^{68}Ga in the atherosclerotic plaques in mice.

Methods

Production of ionic ^{68}Ga

^{68}Ga radionuclide is readily available by elution from a $^{68}\text{Ge}/^{68}\text{Ga}$ generator (Cyclotron Co., Obninsk, Russia) with 0.1 M HCl. The radioactive elution peak, monitored online with a positron-sensitive photodiode detector (Hamamatsu S5591, Hamamatsu Photonics K.K. Solid State Division, Hamamatsu City, Japan), was collected and the ^{68}Ga -chloride was neutralized with 1 M NaOH to give pH value of 7, as described earlier [7]. The quantity of colloidal ^{68}Ga in the final product was measured by ultrafiltration, as indicated by the activity retained on the 0.2- μm ultrafilter. The final ^{68}Ga product contained 13% of colloidal forms of ^{68}Ga .

Ex vivo biodistribution of ^{68}Ga

Nine 10-11-months-old male atherosclerotic LDLR $^{-/-}$ ApoB $^{100/100}$ mice (weight 35 ± 5 g, mean \pm SD) [8,9] and six 2.5-month-old male non-atherosclerotic C57BL/6N control mice (weight 28 ± 1 g) were *ex vivo* investigated. LDLR $^{-/-}$ ApoB $^{100/100}$ mice were kept on a high-fat, Western-type diet (TD 88173, Harlan Teklad) for 3-4 months, starting at 7 months of age. C57BL/6N mice were fed with regular diet. The experiments were approved by the Laboratory Animal Care and Use Committee of the University of Turku, Finland.

^{68}Ga (17 ± 2 MBq) was intravenously administered via a tail vein in non-anesthetized mice. Three hours after injection the mice were sacrificed under deep isoflurane anesthesia by cervical dislocation. Samples of blood and various tissues were excised, patted dry, weighed, and measured for radioactivity using an automatic gamma counter (1480 Wizard 3 $^{\text{rd}}$ Gamma Counter; EG & G Wallac, Turku, Finland) cross-calibrated with a dose calibrator (VDC-202, Veenstra Instruments, Joure, The Netherlands). The radioactivity remaining in the tail was compensated, background counts were subtracted, and the radioactivity decay was corrected to the time of injection. The concentration of the radioactivity accumulated in the various tissues over the 3-h period following ^{68}Ga injection was expressed as a percentage of the injected activity per gram of tissue (% IA/g).

Autoradiography analysis of aortic cryosections

The distribution of ^{68}Ga -radioactivity in the aortic tissue was studied by combining digital autoradiography and

hematoxylin and eosin (HE) staining. The aorta and internal control muscle sample from the same animal were frozen and sequential longitudinal 8- and 20- μm sections were cut with a cryomicrotome at -15°C , thaw-mounted onto microscope slides. The sections were air dried for 5 min and apposed to an imaging plate (Fuji Imaging Plate BAS-TR2025, Fuji Photo Film Co., Ltd., Japan). After an exposure time of 2.5 h, the imaging plates were scanned with Fuji Analyser BAS-5000 (Fuji Tokyo, Japan; internal resolution 25 μm). The 20- μm cryosections were stained with HE and examined for morphology under a light microscope. After carefully co-registration of the autoradiographs and HE images, ^{68}Ga -radioactivities were measured in the following regions of interest (ROIs): (1) plaque (excluding media), (2) healthy vessel wall (no lesion formation), (3) adventitia (including adjacent fat), and (4) muscle (internal control tissue). In control mice, no plaque areas were seen and ROIs were defined for healthy vessel wall, adventitia, and muscle. In each mouse, the uptakes of ^{68}Ga -radioactivities in the regions of interest were calculated and normalized against internal control tissue (muscle). The results of digital autoradiography analysis were expressed as photostimulated luminescence per square millimeter (PSL/ mm^2).

Assessment of degree of inflammation in atherosclerotic plaques

Immunohistochemical staining with the mouse macrophage specific antibody (Mac-3, clone m3/84, BD Pharmingen, BD550292, USA - BD Biosciences Pharmingen, Franklin Lakes, NJ, USA) was performed using aortic longitudinal 8- μm cryosections in order to detect activated macrophages, as described earlier [10]. Based on the Mac-3 staining, plaque areas were divided into four categories for the semiquantitative estimation of the degree of plaque inflammation; (1) no inflammation = no macrophages, (2) mild inflammation = occasional macrophages, (3) moderate inflammation = occasional and some groups of macrophages, (4) severe inflammation = abundant infiltration of macrophages. The uptake of ^{68}Ga -radioactivity in the different categories was studied with digital autoradiography from 8- μm cryosections combined with images of Mac-3 immunostained sections. The results of digital autoradiography analysis were normalized against internal control tissue (muscle) and expressed as PSL/ mm^2 .

In vivo imaging

Three additional female LDLR $^{-/-}$ ApoB $^{100/100}$ mice, aged 14 to 15 months and kept on a high-fat, Western-type diet for 5 to 6 months (weight 36 ± 10 g, mean \pm SD) were *in vivo* imaged with the Inveon small animal PET/CT scanner (Siemens Medical Solutions,

Knoxville, TN, USA) at 3 h after injection of ^{68}Ga (16 ± 3 MBq). PET images were acquired for 15 min, followed by CT angiography (10 min) without moving the animal. To obtain vascular contrast, 0.2 ml of iodinated intravascular contrast agent eXIATM160XL (Binitio Biomedical Inc, Ottawa, ON, Canada) was injected. CT acquisition consisted of 270 projections acquired with exposure time of 400 ms, x-ray voltage of 80 kVp, and anode current of 400 μA for a full 360° rotation. Mice were kept fully sedated with 1.5% isoflurane during imaging. PET image was reconstructed using OSEM3D algorithm. The resulting matrix was 128×128 pixels with 159 transverse slices in a transaxial field of view of 12.7 cm (pixel size $0.87 \times 0.87 \times 0.80$ mm). CT image was reconstructed using a modified Feldkamp algorithm. The resulting matrix was 256×256 pixels with 384 transverse slices (pixel size $0.17 \times 0.17 \times 0.17$ mm). Co-registration of PET and CT images was done using an automatic weighted mutual information algorithm and confirmed visually on the basis of anatomical landmarks. Quantitative PET analysis was performed by drawing ROIs of the same size in the left ventricle (blood pool), aortic arch, and brachiocephalic artery as identified on the basis of the CT angiography by using the Inveon Research Workplace software (Siemens Medical Solutions, Knoxville, TN, USA). Radioactivity concentrations were corrected for injected radioactivity, and the results were expressed as percentage of injected radioactivity per gram of tissue (% IA/g) assuming 1 mL equals 1 g.

Statistical methods

All the results are expressed as mean \pm SD. Student's *t*-test and one-way ANOVA were applied when comparing the biodistribution results of the atherosclerotic and control mice. *T* test with a mixed Dunnett's model was used to correct the *p* values of biodistribution of aortic uptake versus different tissue uptakes in the atherosclerotic and control mice groups. In the autoradiographic analysis, a mixed model with Tukey-Kramer corrected *p* values was applied to individual mean values of ROIs. A *p* value less than 0.05 was considered as statistically significant.

Results

Characterization of atherosclerotic plaques

After 3 to 4 months on a Western-type diet, the $\text{LDLR}^{-/-}\text{ApoB}^{100/100}$ mice had developed areas covered with atherosclerotic plaques in aortic arch, aortic arteries, and also in the distal part of aorta. Histologically, the plaques were of fibroatheroma type and some of them contained calcifications. In the aortas of the control mice, no atherosclerotic plaques were detected.

Ex vivo biodistribution of ^{68}Ga -radioactivity

The biodistribution of ^{68}Ga -radioactivity at 3 h after i.v. injection is shown in Table 1. The highest level of ^{68}Ga -radioactivity was found in the blood in both mouse strains. The uptake in the whole aorta was higher in $\text{LDLR}^{-/-}\text{ApoB}^{100/100}$ mice than in control mice, but the difference did not reach statistical significance. The aorta/heart and aorta/blood uptake ratios were 1.6 ± 0.7 and 0.2 ± 0.1 in atherosclerotic mice and 1.2 ± 0.2 and 0.2 ± 0.1 in control mice, respectively. The measured radioactivities in the bone and liver of atherosclerotic mice were significantly lower than in the control mice.

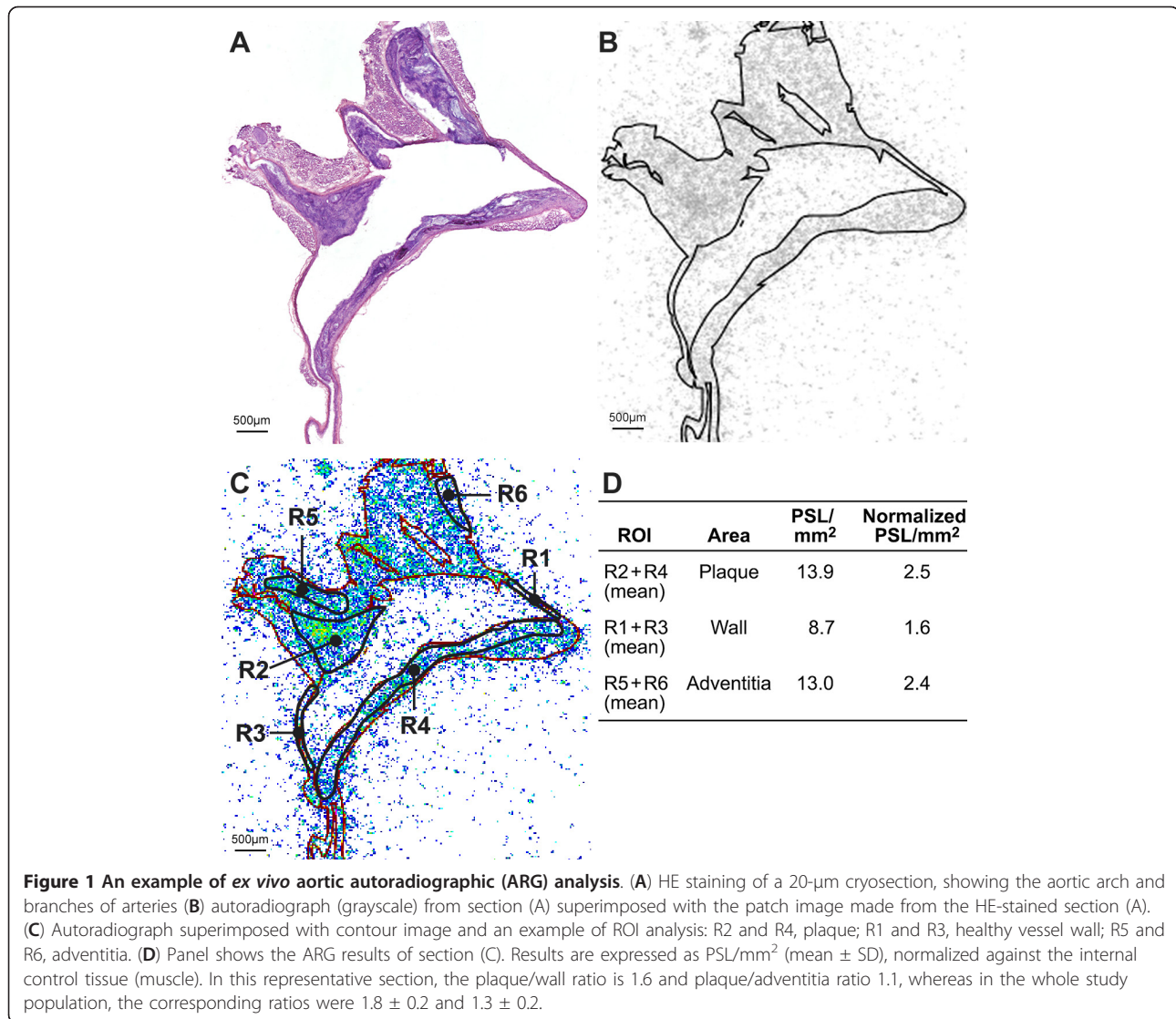
Digital autoradiography of aortic cryosections

A total of 8 to 12 autoradiographs of aortic cryosections from eight $\text{LDLR}^{-/-}\text{ApoB}^{100/100}$ mice (one sample was discarded from the analysis because of remaining blood clot inside the aorta) and 8 autoradiographs of aortic sections from six control mice were generated and superimposed on corresponding digitalized HE staining images. In total, 1,208 ROIs (plaque *n* = 384, healthy vessel wall *n* = 396, adventitia *n* = 406, muscle *n* = 56) were analyzed from 14 mice. The autoradiography analysis revealed a significantly higher uptake of ^{68}Ga -radioactivity in plaques compared with healthy vessel wall (3.4 ± 0.6 vs. 1.9 ± 0.3 PSL/ mm^2 , *p* = 0.0002) and adventitia (3.4 ± 0.6 vs. 2.6 ± 0.3 PSL/ mm^2 , *p* = 0.0011). The plaque/wall ratio was 1.8 ± 0.2 and plaque/adventitia ratio 1.3 ± 0.2 in $\text{LDLR}^{-/-}\text{ApoB}^{100/100}$ mice (Figure 1). The difference between the adventitia and the healthy

Table 1 Ex vivo biodistribution of radioactivity in atherosclerotic $\text{LDLR}^{-/-}\text{ApoB}^{100/100}$ and C57BL/6N control mice

	$\text{LDLR}^{-/-}\text{ApoB}^{100/100}$ (<i>n</i> = 9, urine <i>n</i> = 8)	C57BL/6N (<i>n</i> = 6, urine <i>n</i> = 5)	<i>p</i> value
Aorta	1.99 ± 0.73	1.52 ± 0.40	NS ^a
Bladder	2.50 ± 0.62	1.92 ± 0.29	NS
Blood	8.60 ± 1.29	8.07 ± 0.55	NS
Bone	2.25 ± 0.50	4.08 ± 0.49	< 0.05
Fat	0.46 ± 0.21	0.51 ± 0.07	NS
Heart	1.26 ± 0.26	1.29 ± 0.20	NS
Intestine	2.71 ± 0.70	3.16 ± 0.36	NS
Kidney	4.07 ± 0.78	4.25 ± 0.33	NS
Liver	2.69 ± 1.14	8.34 ± 4.33	< 0.05
Lungs	3.28 ± 1.10	3.58 ± 0.33	NS
Lymph nodes	2.03 ± 0.51	2.35 ± 0.34	NS
Muscle	0.71 ± 0.24	0.71 ± 0.08	NS
Pancreas	1.21 ± 0.25	1.48 ± 0.21	NS
Spleen	3.20 ± 1.28	4.51 ± 1.63	NS
Thymus	1.89 ± 0.96	1.18 ± 0.15	NS

At 3 h after intravenous injection of ionic ^{68}Ga . Results are expressed as % IA/g (mean \pm SD). NS, not significant. ^aDifference between atherosclerotic and control mice.



vessel wall was not statistically significant in either of the mouse strains. A relatively high uptake of ⁶⁸Ga-radioactivity was detected in the calcified areas ($n = 55$ from the total 384 plaque ROIs) of atherosclerotic plaques vs. healthy vessel wall (ratio 2.1 ± 0.6 , $p = 0.0010$). Calcified areas did not contain any macrophages. No statistically significant difference was detected in calcified areas of plaques vs. non-calcified plaques. The variability of the used digital autoradiography analysis has been tested and described earlier [10].

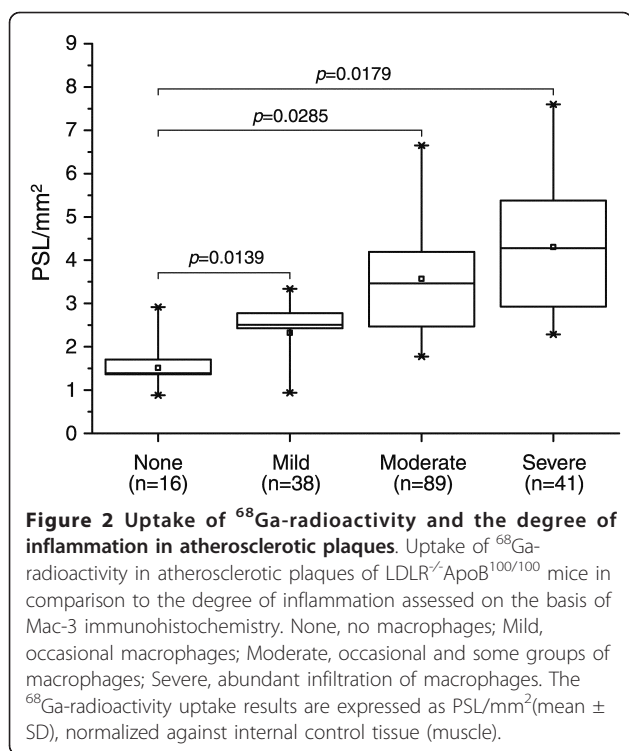
Assessment of ⁶⁸Ga-radioactivity uptake in macrophage-rich areas of atherosclerotic plaques

A total of 184 plaques obtained from four aortic cryosections of each $LDLR^{-/-}ApoB^{100/100}$ mouse were analyzed and normalized against internal control tissue (muscle). According to the autoradiographic analysis,

the uptake of ⁶⁸Ga in plaques with different degrees of inflammation was 1.5 ± 0.7 PSL/mm² in non-inflamed plaques ($n = 16$), 2.3 ± 0.8 PSL/mm² in mildly inflamed plaques ($n = 38$), 3.6 ± 1.5 PSL/mm² in moderately inflamed plaques ($n = 89$), and 4.3 ± 1.9 PSL/mm² in severely inflamed plaques ($n = 41$). Figure 2 shows the co-localisation of the ⁶⁸Ga-radioactivity uptake and degree of macrophage-rich areas in atherosclerotic plaques. Representative Mac-3 stainings of non-inflamed and severely inflamed plaques are shown in Figure 3.

In vivo imaging

In vivo PET/CT imaging demonstrated high radioactivity in the blood pool ($8.1 \pm 2.2\%$ IA/g, $n = 3$) at 3 h after ⁶⁸Ga injection as seen in the aorta and heart of $LDLR^{-/-}ApoB^{100/100}$ mouse (Figure 4). The *in vivo* uptake of



^{68}Ga -radioactivity in the aortic arch and brachiocephalic artery was 6.4 ± 3.0 and $5.8 \pm 2.5\%$ IA/g, respectively.

Discussion

Macrophages play a crucial role in the progression and development of atherosclerosis from early fatty-streak lesions to advanced atherosclerotic plaques [11]. Ruptured plaques, in particular, commonly contain high quantities of macrophages [3]. Therefore, the contents of macrophages may be an excellent imaging biomarker for the vulnerability of atherosclerotic plaques. The present results revealed that the ^{68}Ga -radioactivity uptake in atherosclerotic plaques, especially in their macrophage-rich areas, was higher when compared to healthy vessel wall. This observation strengthens our conception that ^{68}Ga -radioactivity accumulates at the site of inflammation.

^{68}Ga radionuclide is readily available by elution from a $^{68}\text{Ge}/^{68}\text{Ga}$ generator with 0.1 M HCl in the form of ^{68}Ga -chloride. However, after neutralization, ^{68}Ga -chloride is hydrolyzed *in situ* or after administration *in vivo*. In general, ionic $^{68}\text{Ga}^{3+}$ is in the form of soluble anion called gallate, $^{68}\text{Ga}(\text{OH})_4^-$, and/or insoluble colloidal particles $^{68}\text{Ga}(\text{OH})_3$. In the present study, the final ^{68}Ga product contained 13% of colloidal forms of ^{68}Ga . Uncharged gallium hydroxide or gallium nanoparticles are capable of penetrating the cell. Under the lower pH conditions, inside the cell, the material ionizes and becomes bound. Accordingly, accumulation into the

liver, spleen, and bone marrow would be expected [12,13].

In blood, ^{68}Ga -radioactivity can circulate also as a free $^{68}\text{Ga}^{3+}$ and mimic ferric ions. In spite of their physical similarities, gallium and iron behave differently *in vivo*. The major difference is the inability of gallium to be reduced *in vivo* wherefore gallium remains bound to iron-transport proteins and carrier molecules with the inability to interact with protoporphyrin IX to form heme. A high blood uptake of gallium is explained by its binding to iron-binding molecules; transferrin, lactoferrin, and ferritin. One way to facilitate the solubilization of ^{68}Ga may be its chelation with citrate. For SPECT imaging, ^{67}Ga is indeed administrated as citrate to avoid protein binding. Since citrate is only a weak chelator *in vivo*, ^{67}Ga is rapidly released, hydrolyzed, and bound to transferrin and other iron-binding proteins [12,14-16], suggesting that chelation does not improve the uptake of the tracer. We have compared uptakes of ^{68}Ga and ^{68}Ga -citrate in rat osteomyelitis model (unpublished data), and ascertained that there were no differences between ^{68}Ga and ^{68}Ga -citrate uptakes in inflammation lesions.

In comparison to ^{67}Ga -based SPECT, ^{68}Ga -based PET may have some advantages, such as a better resolution for the detection of inflammation and a smaller radiation exposure for the subject. However, the blood clearance of ^{68}Ga -radioactivity was slow as demonstrated by *ex vivo* measurement and by *in vivo* PET/CT imaging. Unfortunately, the relatively short half-life of ^{68}Ga does not allow delayed imaging times for better blood clearance. In an inflamed lesion, ^{67}Ga is accumulated in the areas rich in infiltrated macrophages. Interestingly, ^{67}Ga is not accumulated at the sites of crowded neutrophils, suggesting that the polymorphonuclear leukocytes do not play a major role in the accumulation of ^{67}Ga in inflammatory lesions [17].

In the present study, the plaque/wall ratio of ^{68}Ga was 1.8 ± 0.2 . As compared to 2-deoxy-2- ^{18}F fluoro-D-glucose (^{18}F -FDG), we have measured the plaque/wall ratio of 2.7 ± 1.1 approximately in the same aged $\text{LDLR}^{-/-}\text{ApoB}^{100/100}$ mice as used in the present study [18]. It has been shown that the clinical image qualities of ^{68}Ga -tracers ($\beta +$ decay 97%, $E\beta +$ max 0.64 MeV) and ^{18}F -tracers ($\beta +$ decay 97%, $E\beta +$ max 0.64 MeV) are not necessarily very much different from each other [19]. However, ^{68}Ga has a higher kinetic energy compared to ^{18}F , which could decrease the imaging spatial resolution, particularly when a small plaque lesion is imaged with a high resolution small PET/CT. Based on these earlier observations, ^{18}F -FDG seems to be more promising PET tracer for imaging of atherosclerotic plaques than ^{68}Ga .

Clinical observations indicate that in normal circumstances, the major proportion of the gallium retained in

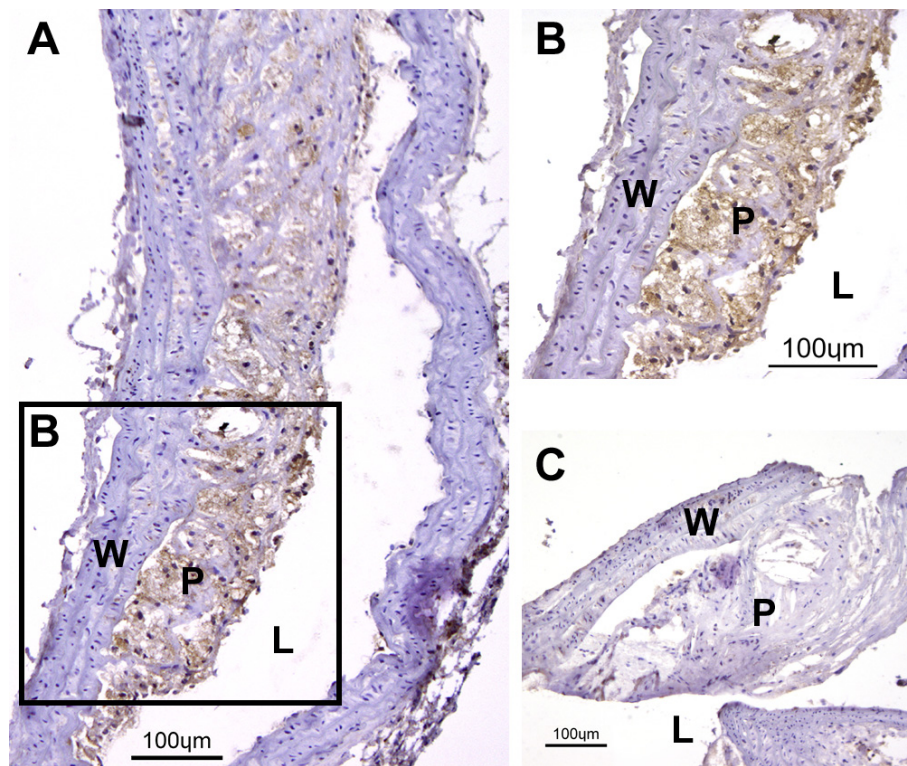


Figure 3 Mac-3 immunostained atherosclerotic plaques. (A) Representative Mac-3 immunostainings of severely inflamed plaque. Macrophages are shown in brown color. Adventitia and healthy vessel wall areas were Mac-3 negative. (B) An enlarged area rich in macrophages marked in (A). (C) Non-inflamed plaque with only scanty immunopositivity for Mac-3. L, lumen; P, plaque; W wall.

the body is localized in the bone and liver, and that inflammatory lesions alter this biodistribution, frequently causing decreased hepatic uptake [15]. In the present study, a difference in the uptake of ^{68}Ga between the atherosclerotic mice and controls was found in bone and liver. The uptake of ^{68}Ga -radioactivity in the whole aorta of atherosclerotic mice was higher than that in the control mice, but the difference was not

significant. The uptake in the inflammatory plaques could partly explain the lower uptake of ^{68}Ga in the liver of atherosclerotic mice. More likely this may be due to liver failure caused by high fat content, which can occur in older $\text{LDLR}^{-/-}\text{ApoB}^{100/100}$ mice fed with a Western-type diet. Concerning the uptake of ^{68}Ga in the bone, we assume that in the young control mice (aged 2.5 months), active bone remodeling may have

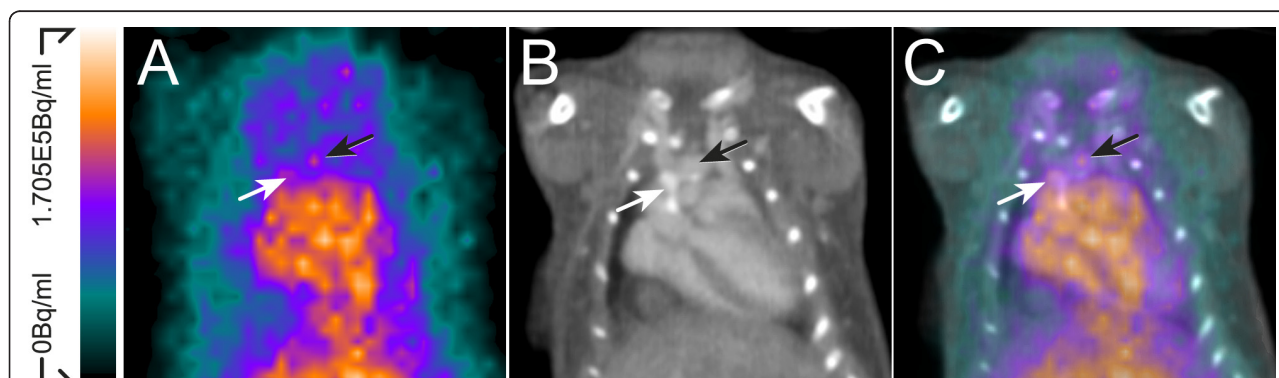


Figure 4 In vivo imaging. (A) *In vivo* PET, (B) CT angiography, and (C) fused PET/CT images demonstrate the high ^{68}Ga signal in the blood pool as seen in the aorta and heart. Calcified (white arrows) and non-calcified (black arrows), aortic arch and aortic root can be seen in contrast-enhanced CT angiography.

contributed to the higher bone uptake as compared to the older LDLR^{-/-}ApoB^{100/100} mice (aged 10 to 11 months).

The accumulation of ⁶⁸Ga-radioactivity in inflammatory lesions is complex, and the majority of ⁶⁸Ga is probably delivered into the inflammatory lesions through the increased permeability at the site of atherosclerotic arteries. In the present study, accumulated ⁶⁸Ga-radioactivity was detected in the macrophages-rich plaques suggesting that ⁶⁸Ga accumulates at the site of inflammation. In addition to that, calcified areas of atherosclerotic plaques were also detected by ⁶⁸Ga, which may be explained by the competitive binding of gallium ions to the Ca²⁺ and Mg²⁺ binding sites [17]. Since the calcified areas can be localized with CT, this observation is not limiting the use of ⁶⁸Ga to distinguish macrophages-rich plaques and calcified plaques.

To some extent, gallium may also be taken up by atherosclerotic plaques due to its binding to the circulating transferrin and avidly to the transferrin receptors at the site of atherosclerotic arteries. Transferrin receptor expression has been shown to correlate positively with macrophage infiltration in human carotid atherosclerotic lesions [20]. Moreover, symptomatic patients with carotid atherosclerosis have significantly higher expression of transferrin receptors than asymptomatic patients [21]. However, although the uptake of ⁶⁸Ga in inflamed atherosclerotic plaques was promising as measured by autoradiography, the slow blood clearance limits the use of ionic ⁶⁸Ga for *in vivo* imaging of atherosclerotic plaques.

Conclusions

Autoradiography analysis showed a moderate, but significantly higher ⁶⁸Ga-radioactivity uptake in the aortic plaques of atherosclerotic mice, especially at the sites rich in macrophages, as compared to areas of healthy vessel wall. While the uptake of ⁶⁸Ga-radioactivity was prominent in the atherosclerotic plaques of LDLR^{-/-}ApoB^{100/100} mice, the slow blood clearance limits the feasibility of ionic ⁶⁸Ga for clinical imaging of atherosclerotic plaques especially in coronary arteries.

Acknowledgements

The authors would like to thank Erja Mäntysalo and Erica Nyman for technical assistance, and Ville Aalto for statistical analyses. This work was funded by the Instrumentarium Foundation, the Finnish Cultural Foundation, the Finnish Foundation for Cardiovascular Research, Aarne Koskelo Foundation, and Ida Montin Foundation and it was conducted in the Finnish Centre of Excellence in Molecular Imaging in Cardiovascular and Metabolic Research, supported by the Academy of Finland, the University of Turku, the Turku University Hospital, and the Åbo Akademi University.

Author details

¹Turku PET Centre, University of Turku and Turku University Hospital, Turku, Finland ²Nuklearmedizinische Klinik der Technischen Universität München,

Munich, Germany ³Department of Pathology, Turku University Hospital, Turku, Finland ⁴A. I. Virtanen Institute for Molecular Sciences, University of Eastern Finland, Kuopio, Finland ⁵Turku Center for Disease Modeling, University of Turku, Turku, Finland

Authors' contributions

JMUS contributed the conception and design, performed the experiments, analyzed and interpreted data and drafted the manuscript. IL performed the experiments, acquired, analyzed and interpreted data and participated in writing of the manuscript. HJS prepared the ⁶⁸Ga and participated in writing of the manuscript. VJOL involved in designing the analysis and interpretation of data, and in drafting and revising the manuscript. PL involved in designing the experiments and revising the manuscript. SY-H, JK, and AR contributed the conception and design, critically contributed and revised the manuscript and enhanced its intellectual content. All authors have approved the final content of the manuscript.

Competing interests

The authors declare that they have no competing interests.

Received: 6 July 2011 Accepted: 17 August 2011

Published: 17 August 2011

References

1. Bobryshev YV: Monocyte recruitment and foam cell formation in atherosclerosis. *Micron* 2006, **37**:208-222.
2. Choudhury RP, Lee JM, Greaves DR: Mechanisms of disease: macrophage-derived foam cells emerging as therapeutic targets in atherosclerosis. *Nat Clin Pract Cardiovasc Med* 2005, **2**:309-315.
3. Davies MJ, Richardson PD, Woolf N, Katz DR, Mann J: Risk of thrombosis in human atherosclerotic plaques - Role of extracellular lipid, macrophage, and smooth-muscle cell content. *Br Heart J* 1993, **69**:377-381.
4. Moreno PR, Falk E, Palacios IF, Newell JB, Fuster V, Fallon JT: Macrophage infiltration in acute coronary syndromes - Implications for plaque rupture. *Circulation* 1994, **90**:775-778.
5. Wilson HM, Barker RN, Erwig LP: Macrophages: Promising targets for the treatment of atherosclerosis. *Curr Vasc Pharmacol* 2009, **7**:234-243.
6. Al Nahhas A, Win Z, Szyszko T, Singh A, Khan S, Rubello D: What can gallium-68 PET add to receptor and molecular imaging? *Eur J Nucl Med Mol Imaging* 2007, **34**:1897-1901.
7. Ujula T, Salomäki S, Autio A, Luoto P, Tolvanen T, Lehkoinen P, Viljanen T, Sipilä H, Härkönen P, Roivainen A: Ga-68-chloride PET reveals human pancreatic adenocarcinoma xenografts in rats-comparison with FDG. *Mol Imaging Biol* 2010, **12**:259-268.
8. Dhawan VM, Sziklas JJ, Spencer RP: Localization of Ga-67 in inflammations in absence of circulating polymorphonuclear leukocytes. *J Nucl Med* 1978, **19**:292-294.
9. Heinonen SE, Leppänen P, Kholova I, Lumivuori H, Häkkinen SK, Bosch F, Laakso M, Ylä-Herttua S: Increased atherosclerotic lesion calcification in a novel mouse model combining insulin resistance, hyperglycemia, and hypercholesterolemia. *Circ Res* 2007, **101**:1058-1067.
10. Haukkala J, Laitinen I, Luoto P, Iveson P, Wilson I, Karlsen H, Cuthbertson A, Laine J, Leppänen P, Ylä-Herttua S, Knuuti J, Roivainen A: Ga-68-DOTA-RGD peptide: biodistribution and binding into atherosclerotic plaques in mice. *Eur J Nucl Med Mol Imaging* 2009, **36**:2058-2067.
11. Saha P, Modarai B, Humphries J, Mattock K, Waltham M, Burnand KG, Smith A: The monocyte/macrophage as a therapeutic target in atherosclerosis. *Curr Opin Pharmacol* 2009, **9**:109-118.
12. Hnatowich DJ: Review of radiopharmaceutical development with short-lived generator-produced radionuclides other than Tc-99 m. *Int J Appl Radiat Isot* 1977, **28**:169-181.
13. Mäkinen TJ, Lankinen P, Pöyhönen T, Jalava J, Aro HT, Roivainen A: Comparison of F-18-FDG and Ga-68 PET imaging in the assessment of experimental osteomyelitis due to Staphylococcus aureus. *Eur J Nucl Med Mol Imaging* 2005, **32**:1259-1268.
14. Green MA, Welch MJ: Gallium radiopharmaceutical chemistry. *Nucl Med Biology* 1989, **16**:435-448.
15. Hoffer P: Gallium - Mechanisms. *J Nucl Med* 1980, **21**:282-285.
16. Oyen WJG, Boerman OC, van der Laken CJ, Claessens RA, van der Meer JW, Corstens FH: The uptake mechanisms of inflammation- and infection-localizing agents. *Eur J Nucl Med* 1996, **23**:459-465.

17. Ando A, Nitta K, Ando I, Katsuda S, Tonami N, Hiraki T, Hisada K, Ogawa H: **Ga-67 Accumulation in inflammatory lesion and its mechanism - Comparison with malignant-tumor.** *Eur J Nucl Med* 1987, **12**:560-566.
18. Laitinen I, Marjamäki P, Haaparanta M, Savisto N, Laine VJ, Soini SL, Wilson I, Leppänen P, Ylä-Herttua S, Roivainen A, Knuuti J: **Non-specific binding of [¹⁸F]FDG to calcifications in atherosclerotic plaques: experimental study of mouse and human arteries.** *Eur J Nucl Med Mol Imaging* 2006, **33**:1461-1467.
19. Sánchez-Crespo A, Andreo P, Larsson SA: **Positron flight in human tissues and its influence on PET image spatial resolution.** *Eur J Nucl Med Mol Imaging* 2004, **3**:1: 44-51.
20. Li W, Xu LH, Forssell C, Sullivan JL, Yuan XM: **Overexpression of transferrin receptor and ferritin related to clinical symptoms and destabilization of human carotid plaques.** *Exp Biol Med* 2008, **233**:818-826.
21. Sullivan JL: **Iron and the sex difference in heart-disease risk.** *Lancet* 1981, **1**:1293-1294.

doi:10.1186/2191-219X-1-14

Cite this article as: Silvola et al.: Uptake of ⁶⁸gallium in atherosclerotic plaques in LDLR^{-/-}ApoB^{100/100} mice. *EJNMMI Research* 2011 **1**:14.

Submit your manuscript to a SpringerOpen[®] journal and benefit from:

- ▶ Convenient online submission
- ▶ Rigorous peer review
- ▶ Immediate publication on acceptance
- ▶ Open access: articles freely available online
- ▶ High visibility within the field
- ▶ Retaining the copyright to your article

Submit your next manuscript at ▶ springeropen.com
